ANNALI DI GEOFISICA, VOL. XXXIX, N. 2, March 1996

Shear-wave polarization alignment on the eastern flank of Mt. Etna volcano (Sicily, Italy)

Francesca Bianco, Mario Castellano, Girolamo Milano and Giuseppe Vilardo
Osservatorio Vesuviano, Ercolano, Napoli, Italy

Abstract
Recently, with the improvement of three-component seismic networks, studies revealing anisotropic characteristics in different regions have assumed great interest. In a complex volcanic area like Mt. Etna (Sicily, Italy), the existence of both iso-oriented fault systems and intrusive bodies consisting of olivine and clinopyroxene suggest the presence of anisotropic structures. In order to investigate this we analyzed the physical phenomenon of shear-wave splitting since under certain constraints, shear waves are less sensitive to local heterogeneity. The aims of this paper are: 1) to evaluate if in a structural complex situation like that at Mt. Etna the signal crossing an anisotropic volume could be enhanced in spite of effects due to undirectional properties along the source-receiver path; 2) to investigate the correlations, if any, between polarization direction of the leading shear wave and the patterns of compressive stress acting on the investigated area. Therefore we measured time-delays between the *S*-onsets on the horizontal components of 3D seismograms to reveal the possible seismic anisotropy in the Etnean region; moreover, we analyzed the polarization vector of shear-waves seismic data recorded during a survey carried out in the spring-summer 1988. We found clear evidence of splitting that we attributed to the presence of an anisotropic volume not homogeneously distributed on the eastern slope of Mt. Etna volcano.

Key words *anisotropy – Mt. Etna – polarization – splitting – S-wave*

1. Introduction

The great complexity of Mt. Etna, characterized by the presence of both iso-oriented fault systems and intrusive bodies, suggests the presence of anisotropic regions.

From the seismic point of view, the existence of anisotropic volumes can be revealed by shear wave splitting (birefringence) observations.

The shear-wave birefringence in local earthquakes has been studied in many countries characterized by a wide variety of tectonic regimes. Among them some observations have been carried out in active volcanic regions like Long Valley caldera (Savage *et al.*, 1990), Campi Flegrei and Hawaii (Savage *et al.*, 1989).

Considering that *P*-wave, Love-wave and Rayleigh-wave studies in anisotropic regions are scarce in information compared with shear wave studies (MacBeth and Crampin, 1991), we chose to measure time-delays between the *S*-onsets on the horizontal components of 3D seismograms to reveal the possible seismic anisotropy in the Etnean region; moreover, we analyzed the polarization vector of shear-waves seismic data recorded during a survey carried out in the spring-summer 1988.

2. Data acquisition and processing

The seismicity here analyzed occurred during spring-summer 1988. The seismic network consisted of 22 three-component digital stations installed by Osservatorio Vesuviano and the Institut de Physique du Globe, Paris.

The instruments used were high-dynamic (120 db) Lennartz PCM5800 digital stations operating in trigger configuration and recording on magnetic tape with 125 Hz sampling rate. The seismometers used were short period 1 Hz Mark L4C-3D and 2 Hz Mark L4A-3D, with the longitudinal component in N-S direction, and the transverse one in E-W direction. Even though the seismic network was not planned for anisotropy experiments, all the instruments were calibrated before and after deployment, to ensure that the responses of horizontal seismometers were the same.

The events recorded during the survey were located using the HYPO71 routine (Lee and Lahr, 1975) with a six layer velocity model (for details see Castellano *et al.*, 1993).

In a volcanic area, strong structural heterogeneity may lead to *S*-phase misreading, and in some cases it is not possible to read shear-waves on the seismograms. In order to ensure quality of the analyzing data, we selected events from the recorded seismicity adopting the following criteria:

i) good *S*-phase identification;

ii) events recorded at least at eight stations;

iii) best localization quality:

ERH $\leq$ 1.5 km

ERZ $\leq$ 2.0 km

RMS $\leq$ 0.30 s.

Then each seismogram was visually inspected and those that showed weak or emergent arrivals, as well as those that were off scale or that gave out anomalous traces due to instrumental problems, were rejected.

Finally a further selection was made to account for the range of the shear-wave window.

Shear-wave window (SWW) is the range of incidence at which the interaction with the free surface affects shear-wave in a less critical way (Evans, 1984; Booth and Crampin, 1985). Moreover, Buchbinder and Haddon's theoretical results (1990) indicated that effects of local surface topography are generally not relevant in shear-wave splitting studies, strictly in the range of SWW. In the Etnean area we chose sigma = 0.25 (Poisson ratio) obtaining a theoretical value of SWW = 35°.

By adopting these rules of selection we excluded a certain number of stations of the original deployments from the data-set where the requested conditions were not satisfied, obtaining a data-set constituted by 11 earthquakes and 10 stations. Epicenters and stations selected are shown in fig. 1. The selected seismicity showed a depth between 8 and 25 km, while the range of magnitude was between 2.3 and 3.1. Our analyses concerned the characteristics of shear-wave splitting in the eastern sector, while we were unable to investigate the western and southern sectors of the volcano. The selected events showed *S*-arrivals, neither irregular nor emergent, in a range of incidence of 15°-31°. Since no arrivals were near the edge of the shear-wave window, the local topography, though very uneven, had no first order effects on our data-set.

In order to preserve shear-wave polarization from perturbations due to multipathing effects and scattering, we filtered the seismic records taking into account the dominant frequency of the *S*-wave signal as well as that pertaining to the seismometer and the stability of polarization in the chosen range (Zollo and Bernard, 1989; de Chabalier *et al.*, 1992).

Since the *S*-wavetrains for these events have dominant spectral amplitudes in the range 1-8 Hz, the seismic signals were filtered by a «zero phase-shift» Butterworth digital filter (36 db octave^{-1}), in the band of 1-6 Hz to 1-8 Hz.

The presence of an anisotropic volume causes two kinds of effects that can be measured on shear wave: time-delay between $qS1$ and $qS2$ phases (hereafter TD) and the polarization anomaly of the *S*-wavetrain.

For our purpose, the most accurate identification of the seismic phases is needed in our records; consequently we analyzed waveforms in the polarization domain also controlling *S*-onsets identification and evaluating polarization parameters, like rectilinearity and complanarity (Montalbetti and Kanasewich, 1970; Jurkevics, 1988; Jepsen and Kennet, 1990; Bataille and Chin, 1991; Riviere-Barbier *et al.*, 1992; Suteau-Henson, 1991).

Table I shows the characteristics of the selected data-set.

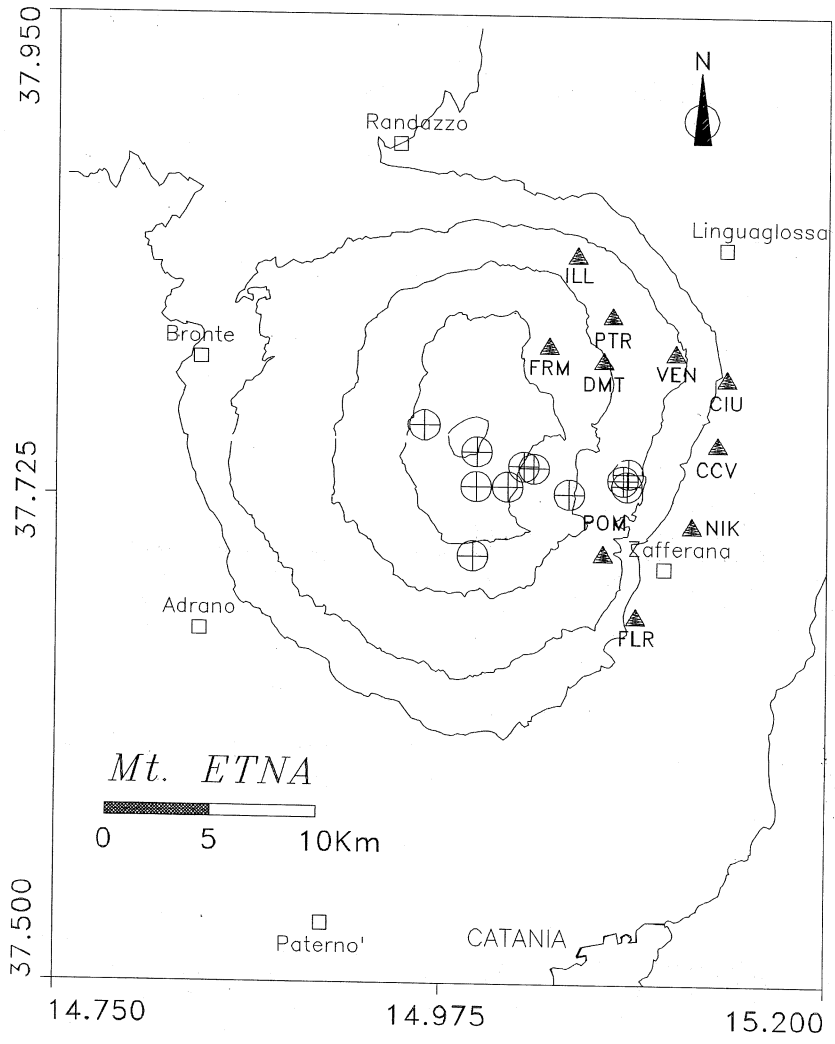

Fig. 1. A map of Mt. Etna: triangles show the location of three-component stations used in our analyses, and the circles represent the epicentral localization of our selected earthquakes.

2.1. *Time-delays*

To ensure the stability of results, our dataset being poor in population, time delay analyses were calculated by means of four different techniques, whose results are in table II:

– visually inspecting the shear-wave traces on a computer screen (table II, column A);

– assuming that the effects of differential attenuation were negligible and that the waveforms were similar, we applied cross-correlation techniques on the unrotated horizontal seismograms (Peron, 1989) (table II, column B);

– assuming the same as the previous point, we applied cross-correlation techniques on the horizontal rotated 5 by 5 degrees seismograms

Table I. Characteristics of the selected data-set.

Station	No. of events	Magnitude	Depth (km)	Incidence
CCV	3	2.4 ÷ 2.5	7.5 ÷ 8.4	15° ÷ 26°
CIU	7	2.4 ÷ 3.1	7.5 ÷ 23.4	15° ÷ 26°
DMT	10	2.3 ÷ 3.1	7.5 ÷ 23.4	15° ÷ 24°
FLR	7	2.4 ÷ 3.1	14.8 ÷ 23.4	16° ÷ 23°
FRM	9	2.3 ÷ 3.1	7.5 ÷ 23.4	15° ÷ 24°
ILL	5	2.3 ÷ 3.1	19.4 ÷ 23.4	19° ÷ 25°
NIK	2	2.4 ÷ 3.1	14.8 ÷ 23.4	20° ÷ 25°
POM	8	2.4 ÷ 3.1	14.8 ÷ 23.4	16° ÷ 22°
PTR	8	2.4 ÷ 3.1	7.5 ÷ 23.4	16° ÷ 31°
VEN	5	2.4 ÷ 3.1	7.5 ÷ 23.4	16° ÷ 28°

(Bowman and Ando, 1987) (table II, column C);

– finally, we estimated TD by measuring the number of points in which the polarization of shear-wave, starting from $qS1$ onset remains linear by diagonalization of covariance matrix using a time moving window of appropriate length (slightly greater than TD measured in previous ways) (table II, column D).

Then we attributed to each station a characteristic TD value that was the weighted mean value of all the TD values estimated for that station. The weighting was based on the following arbitrary number scale:

weight = 1 to visual inspection measures;

weight = 2 to cross-correlation (rotate and unrotate) measures;

weight = 3 to linearity measures.

The weights are in increasing order and the weighted mean values were calculated using the following relation

$$\overline{TD} = \frac{\sum_{i=1}^{N} p_i x_i}{\sum_{i=1}^{N} p_i}$$

where: N = number of measures; x_i = TD measures; p_i = weight of the i-TD measure.

The results of these analyses are in fig. 2, where the weighted mean values at each station are reported; the figure also shows the spatial distribution of the R parameter defined in the next section.

2.2. *Polarization vector*

Studies of polarization anomaly are less influenced by the structural heterogeneity not related to anisotropy than the delay times method (Chen *et al.*, 1987; Crampin, 1981, 1985).

Polarization anomalies have been evidenced by analyzing the time behaviour of the polarization eigenvector in the horizontal plane. This approach, generally used in optical birefringence, is based on the diagonalization of the covariance matrix (Born and Wolf, 1965; Montalbetti and Kanasewich, 1970), is rather similar to what Aster *et al.* (1990) suggested, and has the advantage of computing the eigenvector using the 3D signal even if the representation is 2D. This could lead to more stable results in a very heterogeneous medium (Aster *et al.*, 1990). The difference from the method of Aster *et al.* (1990) consists in the use of polarization eigenvectors not only to infer the polarization direction of $qS1$ phases, but also to study the temporal behaviour of S-wave polarization anomalies.

The diagonalization of the covariance matrix was calculated using an analytical time-moving window across the entire S-phases contained in the recorded signal. We evaluated the duration of the window after estimating the mean value of the linearity interval (the time in which the *qS1* phase is the only wave recorded) choosing, then, the length of the moving window greater than this value, resulting generally 0.5 s. So we compared the results

Table II. TD measurements by four different techniques (see text for explanations) at each station. For each event the time of occurence and the depth are reported.

Station	HH:MM	Z (km)	A	B	C	D
DMT	17:21	8.46	0.07	0.02	0.05	0.08
	17:57	7.53	0.05	0.06	0.05	0.07
	05:54	8.46	0.06	0.05	0.06	0.08
	15:24	17.48	0.06	0.04	0.02	0.10
	03:44	22.38	0.05	0.05	0.06	0.12
	03:56	23.42	0.04	0.05	0.07	0.12
	04:27	21.70	0.03	0.04	0.06	0.09
	06:48	19.45	0.03	0.04	0.07	0.07
	07:02	19.72	0.04	0.10	0.02	0.06
	08:37	15.94	0.04	0.04	0.06	0.05
CCV	17:21	8.46	0.22	0.06	0.07	0.05
	17:57	7.53	0.20	0.08	0.06	0.07
	05:54	8.46	0.07	0.06	0.04	0.03
FLR	19:02	14.80	0.01	0.03	0.03	0.03
	15:24	17.48	0.02	0.03	0.03	0.06
	03:44	22.38	0.03	0.02	0.02	0.03
	03:56	23.42	0.04	0.02	0.02	0.04
	04:27	21.70	0.04	0.02	0.02	0.02
	06:48	19.45	0.05	0.03	0.02	0.02
	07:02	19.72	0.03	0.04	0.06	0.14
	08:37	15.94	0.05	0.02	0.02	0.02
ILL	03:44	22.38	0.09	0.02	0.09	0.01
	03:56	23.42	0.09	0.11	0.02	0.02
	04:27	21.70	0.02	0.04	0.18	0.06
	06:48	19.45	0.04	0.05	0.04	0.03
POM	19:02	14.80	0.03	0.02	0.03	0.02
	15:24	17.48	0.06	0.09	0.05	0.02
	03:44	22.38	0.04	0.08	0.06	0.06
	03:56	23.42	0.04	0.07	0.06	0.07
	04:27	21.70	0.05	0.02	0.03	0.08
	06:48	19.45	0.08	0.10	0.13	0.09
	07:02	19.72	0.03	0.10	0.08	0.09
	08:37	15.94	0.02	0.02	0.02	0.02

Table II (*continued*).

Station	HH:MM	Z (km)	A	B	C	D
	17:21	8.46	0.06	0.03	0.02	0.02
	17:57	7.53	0.04	0.01	0.02	0.04
	05:54	8.46	0.06	0.02	0.02	0.08
	03:44	22.38	0.07	0.05	0.08	0.09
FRM	03:56	23.42	0.12	0.09	0.09	0.08
	04:27	21.70	0.09	0.10	0.03	0.06
	06:48	19.45	0.08	0.08	0.09	0.09
	07:02	19.72	0.01	0.06	0.06	0.09
	08:37	15.94	0.05	0.02	0.01	0.03
	17:21	8.46	0.09	0.09	0.01	0.01
	17:57	7.53	0.06	0.10	0.03	0.02
	05:54	8.46	0.08	0.08	0.09	0.11
CIU	19.02	14.80	0.09	0.06	0.02	0.02
	03:44	22.38	0.02	0.02	0.06	0.07
	03:56	23.42	0.02	0.03	0.06	0.04
	04:27	21.70	0.04	0.03	0.02	0.02
	17:21	8.46	0.07	0.09	0.01	0.01
	17:57	7.53	0.06	0.02	0.01	0.06
VEN	19:02	14.80	0.03	0.06	0.02	0.06
	03:44	22.38	0.04	0.05	0.04	0.06
	03:56	23.42	0.04	0.06	0.03	0.04
	04:27	21.70	0.03	0.05	0.06	0.04
NIK	19:02	14.80	0.03	0.08	0.09	0.10
	03:56	23.42	0.08	0.09	0.09	0.10
	17:21	8.46	0.07	0.07	0.02	0.06
	17:57	7.53	0.07	0.14	0.06	0.02
	05:54	8.46	0.01	0.03	0.02	0.01
PTR	19:02	14.80	0.03	0.02	0.04	0.02
	15:24	17.48	0.03	0.04	0.09	0.03
	03:44	22.38	0.03	0.05	0.06	0.08
	03:56	23.42	0.02	0.06	0.12	0.06
	04:27	21.70	0.03	0.06	0.03	0.09

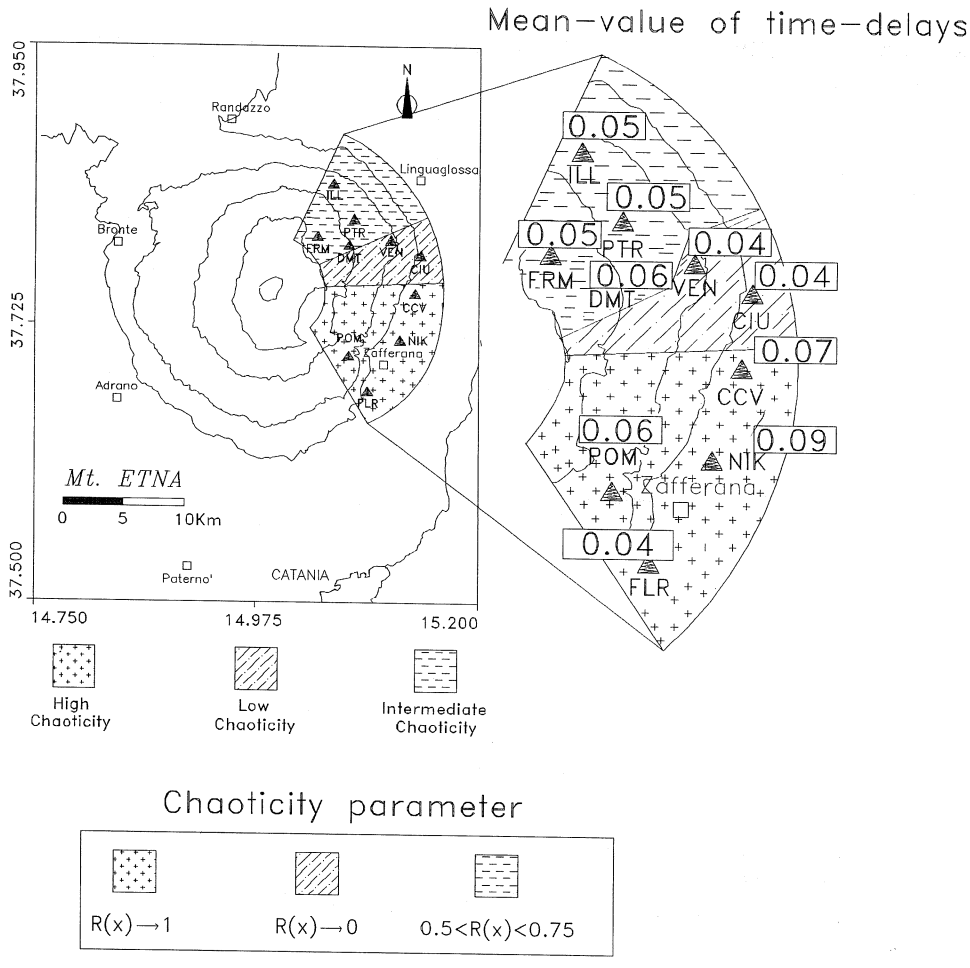

Fig. 2. Subdivision of Mt. Etna's Eastern slope into three sections representing different degrees of anisotropy. On the enlarged picture mean-weighted value of time-delays at each station are reported in the rectangles (see the text for further explanations).

obtained with this technique and those obtained with a widely used 2D representation: the polarigrams. Examples of both polarigram and polarization eigenvector representations are seen in fig. 3a,b.

The observed polarization patterns at different stations are generally less influenced by the hypocenter variation. Therefore, the following results are indicative of the generalized behaviour of the polarization vector at different stations.

Both polarigrams and polarization eigenvectors displayed polarization anomalies. In fact, the polarization anomalies exhibited in the eigenvector representation by means of rotation around *L*-axes, were also revealed in the polarigrams. Although both polarigrams and polarization eigenvectors' behaviour showed the same irregular trend that we call «*chaoticity*», this trend was more evident in the eigenvector representation. For this reason we have

defined an empiric *chaoticity* parameter, that we have called *R(x)*, as: the mean value of the number of rotations of the polarization eigenvectors around the *L*-axis in the time-unity, each value being normalized with respect to the greatest number of rotations in the entire distribution of data-set.

Examples of polarization eigenvectors at different stations are in fig. 4.

This kind of analysis led to the discovery of some interesting behaviour and pointed out a characteristic trend for $R(x)$ starting at POM station, moving counter-clockwise in the northern direction. In fact, we noted a very chaotic polarization eigenvector of the shear waves at POM station. This evidence of polarization anomalies becomes progressively weaker moving towards the northern direction, completely disappearing at VEN station, and gradually reappearing at PTR and ILL stations.

The behaviour of the polarization eigenvectors chaoticity suggested the division of the eastern slope of Mt. Etna into the three sections shown in fig. 2; the figure reports weighted mean-values of estimated TD near each station, and, at the bottom, the behaviour of the chaoticity parameter in each sector. The first section is between stations FLR and CCV, the second one between stations CCV and VEN and the third one between stations VEN and ILL. This subdivision shows good agreement between TD and $R(x)$: the highest values of TD are in the section of the greatest *R(x)* and the lowest values of TD are in the section of the lowest $R(x)$; the correlation coefficient between TD and $R(x)$ is 0.92.

Each section is characterized by a variable degree of splitting, and the highest one is located in the south-eastern section, in accordance with both polarization and time-delay analyses.

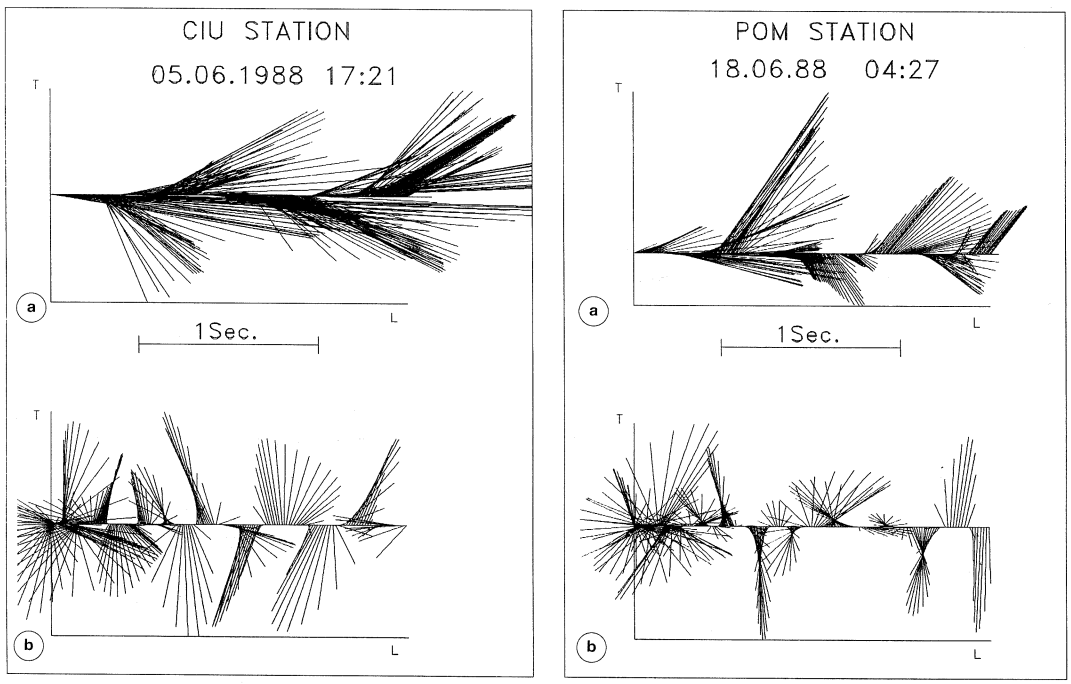

Fig. 3a,b. An example of (a) eigenvector polarization and (b) polarigram representations, both showing polarization anomalies at CIU and POM stations.

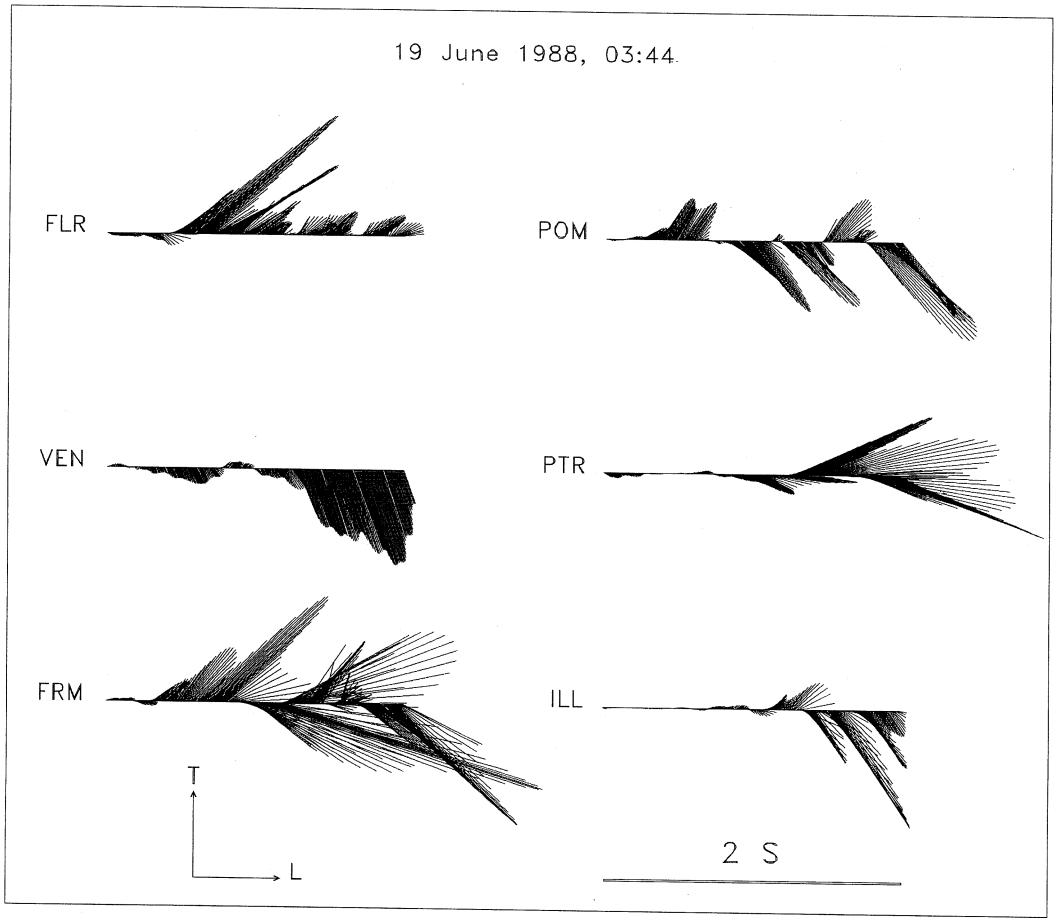

Fig. 4. Different behaviour of polarization eigenvector for June 19th, 1988, 03H44 event at six different stations. Note the chaoticity absence at VEN station and the highest degree of chaoticity at FRM station.

3. Causes of the observed splitting

At this point we analyzed the numerous causes that may have originated the shear-wave splitting, in order to define a physical origin of this phenomenon. We rejected the hypothesis that an *S-P* conversion was responsible for the observed splitting. In fact, in the vertical incidence considered, this type of conversion shows the greatest amplitude on the vertical component; instead, the entire data-set exhibited the maximum amplitude in correspondence with the splitting on the horizontal components (fig. 5). Shear-wave splitting may also have been caused by complex source mechanisms, but due to the low magnitudes of the analyzed events (usually less than 3.0) this hypothesis was rejected as well. Moreover, it was also rejected for the following reasons:

– time delays of each event differed according to the station;

– the events arriving from the same source volume showed the same time-delay signs at each station.

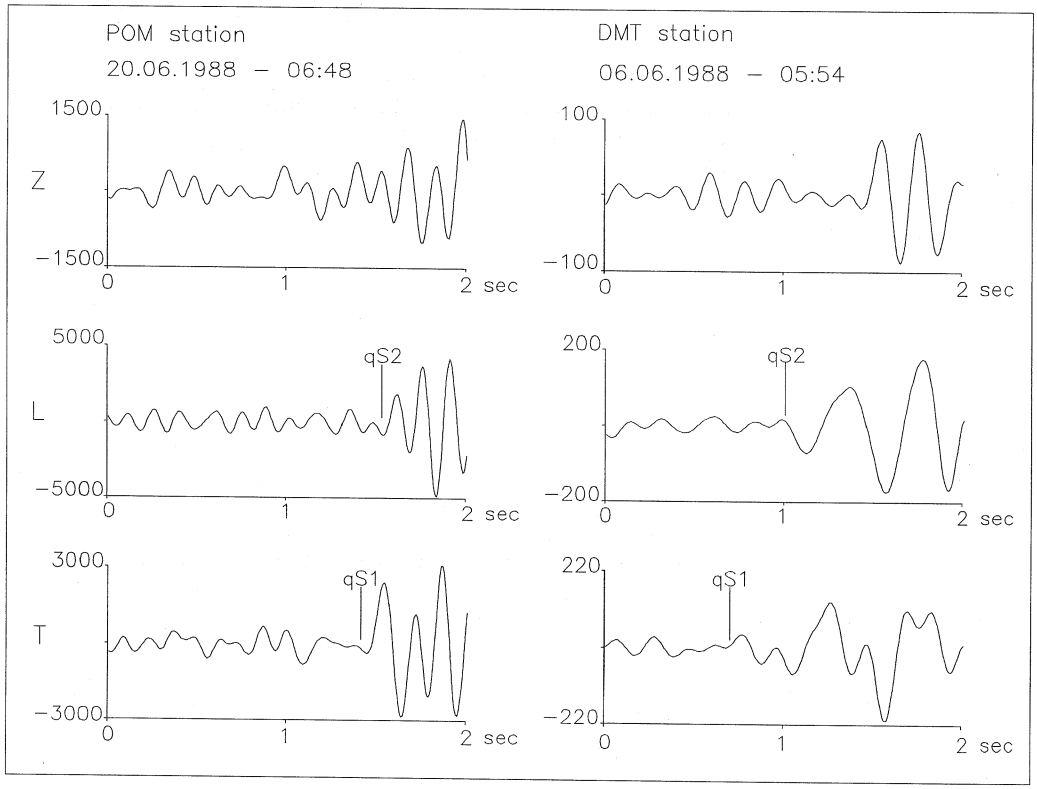

Fig. 5. Two examples of three-component seismograms of shear-waves recorded at two different stations displaying $qS1$ and $q2$ onsets. The amplitudes of the events, in arbitrary units, show that no *S-P* conversion is responsible for the observed splitting because the greatest amplitude for the *S*-phases is on the horizontal components. Both examples are filtered in the 1-8 Hz band.

Furthermore, by changing the events each station showed, on average, different values of time delays, and this leads to the exclusion of site effects.

Consequently, the most probable cause of the observed shear-wave splitting is, in our opinion, the presence of an anisotropic volume with different characteristics not homogeneously distributed on the eastern slope of Mt. Etna volcano. The results of travel time difference analysis suggest that this volume might be concentrated in the upper 15-20 km of the crust.

To evaluate if the observed polarization anomalies were due to the presence of an anisotropic region, we corrected seismic traces by shifting the horizontal components as a function of the time delays. Figure 6a,b also shows the polarization eigenvector analysis performed on the shifted traces. The removal of the anisotropic effect, displayed by the vector parallelism, is especially evident in the first case.

4. Fast shear wave polarization directions

Information on the origin of the observed anisotropic volume could be obtained by $qS1$ polarization directions at each station. In fact if at each station $qS1$ polarization directions, re-

lated to different events, show compatible behaviour, this would confirm the presence of an anisotropic volume under the station. Moreover, if nearby stations show compatible polarization directions, this means that the anisotropic volume has pervasive properties (Munson *et al.*, 1993). Based on Crampin's hypothesis (1981) that crustal anisotropy is generated by parallel alignment of vertical stress-induced microcracks, the direction of the leading shear wave polarization should be parallel to the one of maximum horizontal compressive stress.

Figure 7 reports the mean-value, standard error of $qS1$ polarization eigendirection and number of events at each station. We assumed, empirically, that the range of compatibility for the polarization eigendirections is in 25% fluctuation around the mean-value. This was realized everywhere but at CIU station, which is located in the section we have defined of «low chaoticity», this may further support the fact that the $R(x)$ parameter is related to the degree of splitting. There are no large station-to-station differences in the fast shear-wave polar-

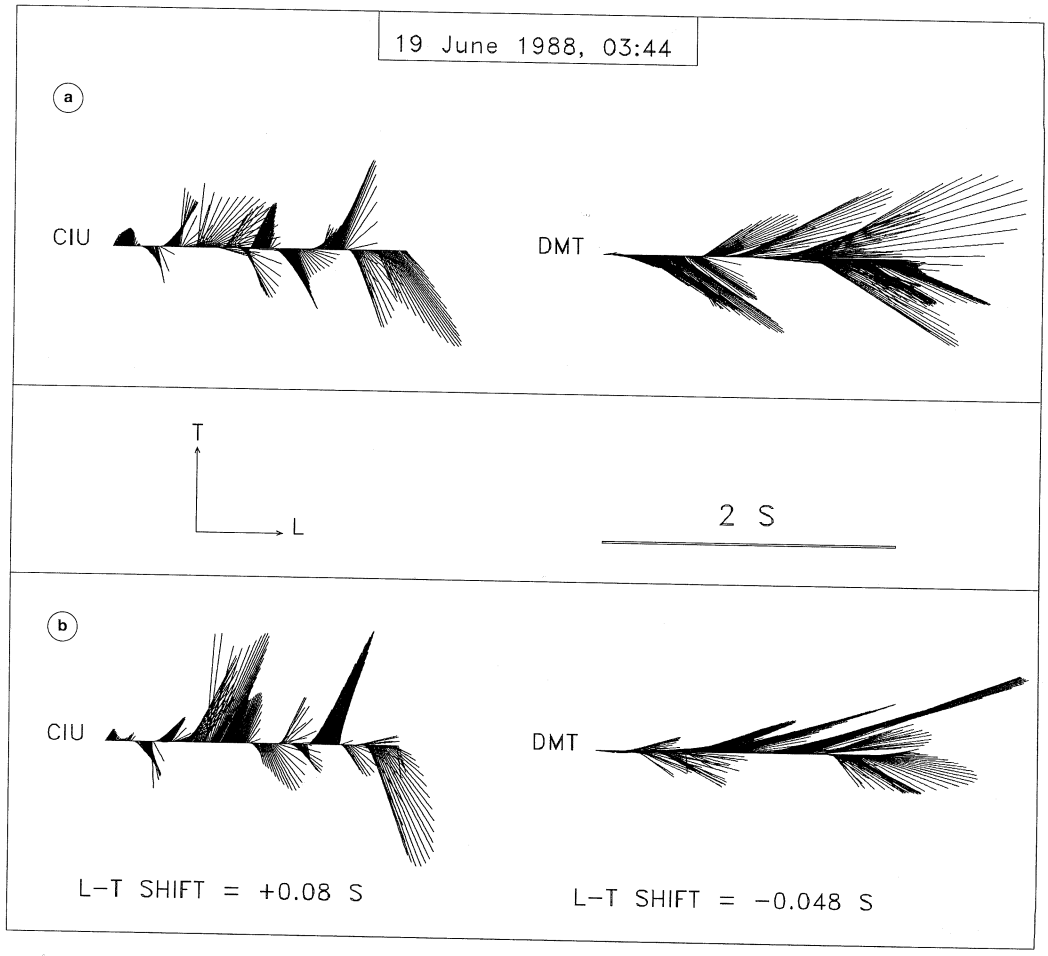

Fig. 6a,b. a) Polarization eigenvectors for June 19th, 1988, 03H44 event at stations CIU and DMT; b) the same eigenvectors corrected for the calculated *L-T* shift reported below.

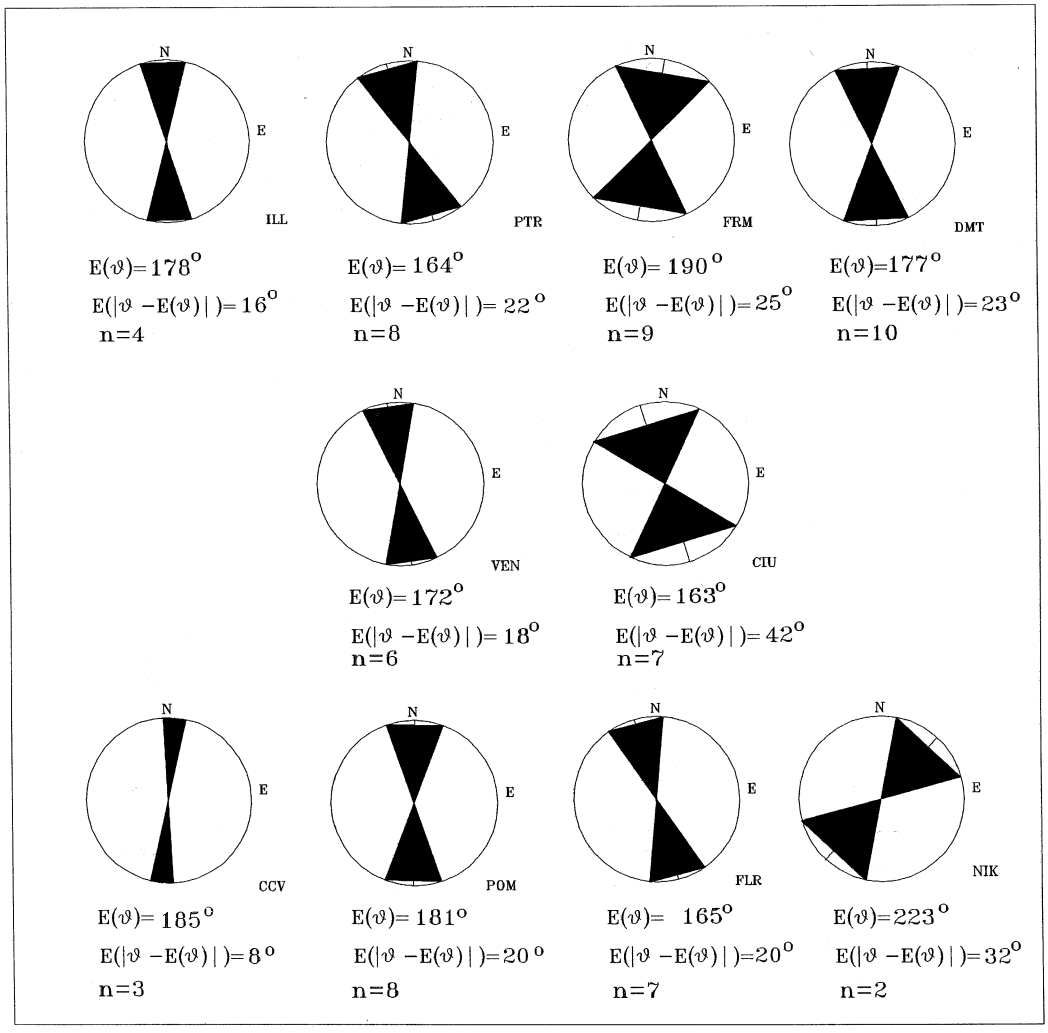

Fig. 7. Mean-value of $qS1$ polarization eigendirections $E(\vartheta)$, standard error $E(|\vartheta - E(\vartheta)|)$ and number of events at each station of the selected data-set.

ization alignments, so we suggest that the heterogeneous anisotropic volume has pervasive features except at FRM and NIK stations where the polarization eigendirections have different alignments with respect to the neighbouring stations.

In order to investigate the causes of the observed anisotropy we compared the polarization directions of the leading shear wave, inferred from the covariance analyses, with both the directions of compressional axes from fault plane solutions of earthquakes recorded during the 1988 experiment and the direction of major surface faults in the area.

Studies of stress regimes on Mt. Etna volcano evidenced the great difficulty in explaining all the structural trends and other information on stress field, like the ones from focal

mechanisms, in a simple model. However it is generally agreed that earthquakes in the shallow crust (depth < 7 km) are characterized by normal faulting processes, while deeper events show a wide variety of mechanisms (*e.g.*, Scarpa *et al.*, 1983). Moreover the maximum horizontal compressive stress results aligned NNE-SSW.

Figure 8 reports mean-values, standard error of eigendirections for each station, as well as the direction of the major fault traces and the mean direction of compressional axis and its

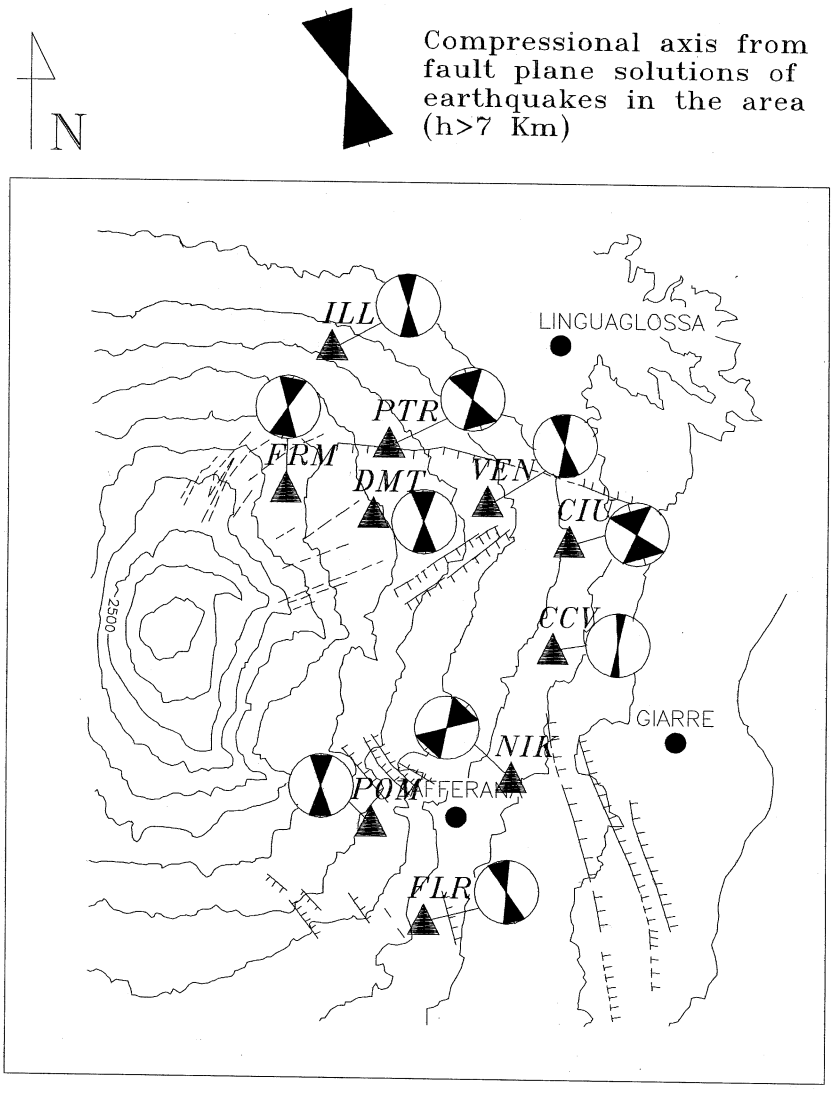

Fig. 8. The same as in fig. 7 compared to the mean-value and standard error of the strike of the compressional axis (at the top) inferred from fault plane solutions of the recorded seismicity and the traces of the major faults in the investigated area.

standard error (in the top), which results compatible with the direction of the regional compressive stress.

In the stress field of the area, cracks or fractures with strike parallel to the maximum compressive stress could be expected to be vertical, perhaps with a broad distribution of dip. The alignment of polarization with compressional axes from fault plane solution may imply that the observations can be interpreted as the effects of shear-wave propagation through the effective anisotropy of distributions of fluid filled cracks and microcracks throughout the rock-mass. In this data-set only one (FRM station) case of orientation parallel to the near-surface fault traces was found, and this should exclude a shallow origin of anisotropy or near-surface site effects, even if a small variation in $qS1$ direction in near stations may be related to small local-effects. Moreover, the irregular topography, even if has only a secondary effect on the recorded polarization, could be taken in account to explain much of the scatter which is apparent in the polarization distribution.

The most evident exception to this behaviour is at NIK station. In this case polarization eigendirections are almost orthogonal to nearby fault traces, but the short number of recorded events precludes any reasonable conclusion.

The exception at FRM station is reasonably related to the fact that this station is located on an active structure named NE Rift, so the $qS1$ polarization eigendirection is aligned in the rift direction.

Moreover, the scatter in data are probably related, again, to the topographic situation, although it may also result from small fluctuations in the crack strikes probably due to local disturbance of stress state.

5. Conclusions

Both polarization and time-delay analyses show clear evidence of shear-wave splitting that seems to be caused by the presence of an anisotropic volume with different characteristics and not homogeneously distributed on the eastern slope of Mt. Etna volcano.

The selected data show a preferred eigendirection of $qS1$ waves in agreement with stress field acting in the area.

These observations suggest that the anisotropic volume might be composed of vertical N-S aligned fluid filled cracks. However, at present we do not have enough data to completely rule out the possibility that observed anisotropy is due to the presence of an intrusive body composed of minerals like olivine and clinopyroxene, clearly observed on Mt. Etna. Moreover, it is possible that both causes may generate anisotropy at the same time.

The result of a travel time difference analysis suggests that the presence of the seismic anisotropy might be concentrated in the upper 15-20 km of the crust. It is to be stressed that the severe constraints adopted to obtain the best events to analyze dramatically reduced the number of statistically significant earthquakes. Consequently our results are not unique and definitive, but preliminary. Much more data over a wide period of different volcanic activity are needed to establish the correlations that seem to exist between shear-wave splitting and stress field on such a complex volcano.

REFERENCES

ASTER, R.C., P. SHEARER and J. BERGER (1990): Quantitative measurements of shear-wave polarization at the Anza seismic network, Southern California: implications for shear-wave splitting and earthquake prediction, *J. Geophys. Res.*, **95**, 12449-12473.

BATAILLE, K. and J.M. CHIU (1991): Polarization analysis of high-frequency, three-component seismic data, *Bull. Seism. Soc. Am.*, **81**, 622-642.

BOOTH, D.C. and S. CRAMPIN (1985): Shear wave polarizations on a curved wavefront at an isotropic free surface, *Geophys. J. R. Astron. Soc.*, **83**, 61-73.

BORN, M. and E. WOLF (1965): *Principles of Optics*, (Pergamon Press, New York), III Edizione, 60-95.

BOWMAN, J.R. and M. ANDO (1987): Shear-wave splitting in the upper mantle wedge above the Tonga subduction zone, *Geophys. J. R. Astron. Soc.*, **88**, 25-41.

BUCHBINDER, G.G.R. and R.A.W. HADDON (1990): Azimuthal anomalies of short period *P*-wave arrivals from Nahanni aftershocks, N.W.T., Canada and effects of surface topography, *Bull. Seism. Soc. Am.*, **80**, 1272-1283.

CASTELLANO, M., F. FERRUCCI, C. GODANO, S. IMPOSA and G. MILANO (1993): Upwards migration of seismic focii: a forerunner of the 1989 eruption of Mt. Etna (Italy), *Bull. Volcanol.*, **55**, 357-361.

CHEN, T., D.C. BOOTH and S. CRAMPIN (1987): Shear-wave polarizations near the North Anatolian fault, III, observations of temporal changes, *Geophys. J. R. Astron. Soc.*, **91**, 287-311.

CRAMPIN, S. (1981): A review of wave motion in anisotropic and cracked elastic-media, *Wave Motion*, **3**, 343-391.

CRAMPIN, S. (1985): Evaluation of anisotropy by shear-wave splitting, *Geophysics*, **50**, 142-152.

DE CHABALIER, J.B., H. LYON-CAEN, A. ZOLLO, A. DESCHAMPS, P. BERNARD and D. HATZFELD (1992): A detailed analysis of microearthquakes in Western Crete from digital three-component seismograms, *Geophys. J. Int.*, **110**, 347-360.

EVANS, R. (1984): Effects of the free surface on shear wavetrains, *Geophys. J. R. Astron. Soc.*, **76**, 165-172.

JEPSEN, D.C. and B.L.N. KENNET (1990): Three component analysis of regional seismograms, *Bull. Seism. Soc. Am.*, **80**, 2032-2052.

JURKEVICS, A. (1988): Polarization analysis of three component array data, *Bull. Seism. Soc. Am.*, **78**, 1725-1743.

LEE, W.H.K. and J.C. LAHR (1975): HYPO71 (revised): a computer program for determining hypocenter, magnitude and first motion pattern of local earthquakes, U.S. Geol. Surv., *Open-File Rep.*, 75-311.

MACBETH, C. and S. CRAMPIN (1991): Comparison of signal processing techniques for estimating the effects of anisotropy, *Geophys. Prosp.*, **39**, 357-385.

MONTALBETTI, J.F. and E.R. KANASEWICH (1970): Enhancement of teleseismic body phases with a polarization filter, *Geophys. J. R. Astron. Soc.*, **21**, 119-129.

MUNSON, C.G., C.H. THURBER and Y. LI (1993): Observations of shear-wave splitting on the southeast flank of Mauna Loa volcano, Hawaii, *Geophys. Res. Lett.*, **20**, 1139-1142.

PERON, J. (1989): Two- and four-component rotation in analysis of shear-wave splitting, presented at *SEG Research Workshop on Recording and Processing Vector and Wavefield data, Snowbird, Utah, August 1989*, 112-113.

RIVIERE-BARBIER, F., A. SUTEAU-HENSON, Z. RYABOY and J.A. CARTER (1992): Analysis of three-component data from Iris/Ida stations in the USSR, *Bull. Seism. Soc. Am.*, **82**, 192-220.

SAVAGE, M.K., X.R. SHIH, R.C. MEYER and R.C. ASTER (1989): Shear-wave anisotropy of active tectonic regions via automated *S*-wave polarization analysis, *Tectonophysics*, **165**, 279-292.

SAVAGE, M.K., W.A. Peppin and U.R. VETTER (1990): Shear-wave anisotropy and stress direction in and near Long Valley caldera, California, 1979-1988, *J. Geophys. Res.*, **95**, 11165-11177.

SCARPA, R., G. PATANÈ and G. LOMBARDO (1983): Space-time evolution of seismic activity at Mt. Etna during 1974-1982, *Annales Geophysicae*, **1**, 451-462.

SUTEAU-HENSON, A. (1991): Three-component analysis of regional phases at Noress and Arcess: polarization and phase identification, *Bull. Seism. Soc. Am.*, **81**, 2419-2440.

ZOLLO, A. and P. BERNARD (1989): *S*-wave polarization inversion of the 15 October 1979; 23:19 Imperial valley aftershock: evidence for anisotropy and a simple source mechanism, *Geophys. Res. Lett.*, **16**, 1047-1050.